A Validation Study of the Four-Pick Point Design Method of a Mobile Crane Rigging Assembly with Over Six Pick Points

Ramy Kheir[1], Sang Hyeok Han[1], Ashutosh Bagchi[1]
[1]Department of Building, Civil and Environmental Engineering, Concordia University, Canada
E-mail: Ramy.kheir@mail.concordia.ca, sanghyeok.han@concordia.ca, ashutosh.bagchi@concordia.ca

Abstract

In the field of modular construction, mobile cranes are an essential tool for lifting large and heavy modules vertically. These modules often need to be lifted without rotation, meaning they must be kept in a flat position during the lifting process to avoid potential structural damage. One of the most important aspects of the lifting process is the rigging design, which consists of components like slings, shackles, and spreader bars. These elements play a vital role in distributing the load during the lifting operation. While considerable progress has been made to automate the rigging design process, the existing methods are often limited in their ability to handle larger lifting configurations involving more than six lifting points. This study addresses these limitations by presenting an in-depth structural analysis verification of the current rigging design method that can be applied to modules with more than six lifting points. The paper provides a detailed step-by-step calculation procedure for all the required components necessary for the design and selection of rigging components. The results presented in this paper represent an important step forward in the development of more advanced methodologies for lifting larger modules with complex rigging requirements, ensuring safety and efficiency.

Keywords –

Rigging assembly; Mobile crane; Pick-points

1 Introduction

In most present heavy lift projects, modularization is adopted as a fast and efficient process where modules are required to be transported to the job sites, lifted from their delivered locations, and set in their final positions. Mobile cranes, set up on the job site, are considered the centerpiece equipment during the on-site module installation phase. Disruptions occurring during this phase can easily take away the benefits of adopting modular construction.

Generally, the modules can weigh up to 160 tons and can come in various sizes of up to 24 ft (7.3 m) in width, 138 ft (42 m) in length, and 27.5 ft (8.4 m) in depth [1]. Modules are categorized into three main types: cable trays, pipe racks, and building modules. These modules may have up to five levels and up to 16 lifting points. The lifted modules should remain in a level position to avoid deflection in the module and/or uneven distribution of the carried load. Rigging failure can result in safety risks, cost overruns, and schedule delays. Cho et al. [2]; MinayHashemi et al. [3] reported that 28.1 % of fatal accidents associated with cranes in the United States were due to the failure of slings, wire ropes, and hoist lines between 2002 and 2012. As rigging assemblies connect the crane's hook to the modules, their slinging arrangement plays a key role in ensuring proper load distribution from the lifting lugs up to the crane's hook. For this reason, a sustainable design method for rigging assemblies with different configurations and sizes is crucial for a safe and efficient module lifting process.

Previously, the common slinging arrangement consisted of a 4-point pick configuration, where four diagonal slings were directly attached between the crane's hook and the pick points. In rare cases when the center of gravity (COG) coincides with the center of mass (COM), an identical length of the four slings transferring the loads from the pick points of the module to the crane's hook was used. In practice, however, sling length adjustments are often required to ensure balanced loads and keep the module horizontal during lifting [3]. Available standards, such as the American Petroleum Institute's API RP2A guidelines [4] and the Det Norske Veritas (DnV) design criteria

[5], can be used for the analysis and design of such rigging assembly configurations. While the former computed the sling loads in a suspended equilibrium condition with a single lump sum safety factor of 4 accounting implicitly for dynamic effects; the latter recommended a load sharing between diagonal slings in a 4-point configuration of 2/3 to 1/3 ratios with a 1.5 Dynamic Amplification Factor (DAF) [6]. Later, Sam [7] developed a spreadsheet solution to find precise load distributions between the four slings, accounting for COG position and variations in sling lengths. [8] performed a non-linear analysis in case when sling lengths tolerances were exceeded due to misfit for computing sling load distributions. Despite the development of these tools, many rigging engineers continue to rely on the trial-and-error method based on their experience and guesswork. While a few commercial design software solutions have been developed to automate the design process, they are not widely adopted due to economic, practical, and technical limitations [3].

A traditional rigging assembly is shown in Figure 1. In these arrangements, triangular slings transfer the load from the lifting points (pick points) to the crane's hook through a series of spreader bars, slings, and shackles found at different levels. The number of lifting points on the module dictates the number of levels in a traditional rigging assembly. In an advanced lift scenario (with 16 points), the total number of inventory components including spreader bars, slings, and shackles can exceed 270. The total rigging configuration height can range between 75 to 165 feet, requiring five assembly levels [3], [9], [10].

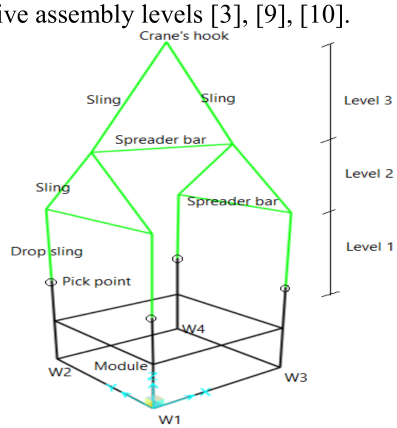

Figure 1. 3D view of a 4-point traditional rigging

Despite the research development presented in MinayHashemi et al. [3] and Hashemi et al. [9], which limited the design process to 6-pick point rigging assemblies, further verification is still required for the current methods used in designing larger rigging configurations with more than six lifting points. This study aims to address that gap and present a more comprehensive verification for the design of rigging systems used in lifting larger modules with up to 16 lifting points.

2 Methodology

2.1 Limitations of the Existing Method (Static Equilibrium)

In 2020, MinayHashemi et al. [3] proposed an automated design framework for analyzing and selecting rigging components in systems with up to four lifting points. This method, while efficient and beneficial for smaller modules, faces significant limitations when applied to larger configurations. The core of this methodology relies on the concept of static equilibrium, which assumes that all forces in the system balance out. This concept works well for smaller systems with simple geometries, but as the number of lifting points increases, the complexity of balancing these forces grows significantly.

2.1.1 First and second levels of 4-pick point configuration

For a system with a 4-point configuration (shown in Figures 1 and 2), the calculations are relatively straightforward. The weight of the module is distributed equally across all lifting points, and the design of the rigging components is based on this assumption. However, when the COG of the module is offset or when the configuration involves more than four lifting points, the situation becomes more complicated. For instance, if a module's COG is not centered, the slings may need to be adjusted in length to balance the forces applied at each lifting point, which may lead to uneven load distribution or the risk of tipping during the lift. For this scenario, the study [3] derived 4 equations (1), (2), (3), and (4) to analyze left sling forces at the first and second levels (FL_1, and FL_2) and the right sling forces at the first and second levels (FR_1 and FR_2) as shown in Figure 2.

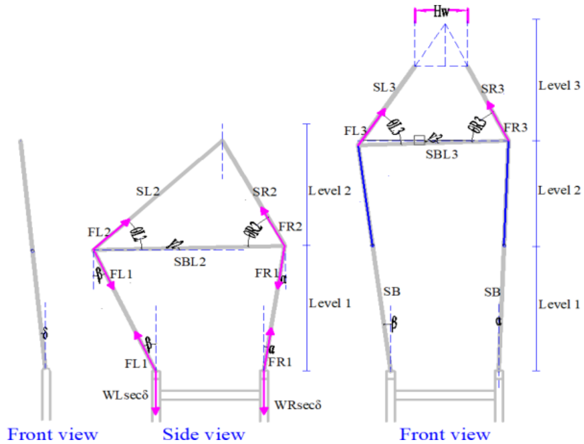

Figure 2. Front and side views of a 4-pick point rigging arrangement with sling internal forces

$$FL_1 = (WL + WR)\sec\delta\csc(\alpha+\beta)\,sin\alpha \tag{1}$$
$$FR_1 = (WL + WR)\sec\delta\csc(\alpha+\beta)\,sin\beta \tag{2}$$
$$FL_2 = (WL + WR)\sec\delta\cos(\theta R-\gamma)\csc(\theta L + \theta R) \tag{3}$$
$$FR_2 = (WL + WR)\sec\delta\cos(\theta L+\gamma)\csc(\theta L + \theta R) \tag{4}$$

For all the equations in this study, the letters L and R represent respectively left and right sides of the assembly. WL and WR are respectively the left and right weight load forces applied at the 2 pick points in the plane containing the drop slings and the spreader bars in the global Y-direction. α and β are the respective right and left drop sling angles with the vertical. θR and θL are respectively the right and left sling angles at the second level. δ is the angle between the plane containing the spreader bar and the 2 above slings in the Y-direction at either the left or the right side of the assembly with the vertical plane. γ is the slope of the spreader bar at the second level in either side plane.

2.1.2 Third level of 4-pick point configuration

Following the sling force computations at the first and second levels, the analysis of the third-level components was conducted in a 2D plane (XZ) containing the spreader bar and the two diagonal slings acting above it using the same method [3] . However, these computations were not shown in that same paper. Here, a detailed analysis of the two sling forces using the free-body diagram of the spreader bar at the third level was performed. Figure 3 presents the free-body diagram of the spreader bar at level 3. Equilibrium equations in both directions were applied to find the required capacity of the two slings and the mounted shackles at the third level. The results are presented in Equations (5) and (6).

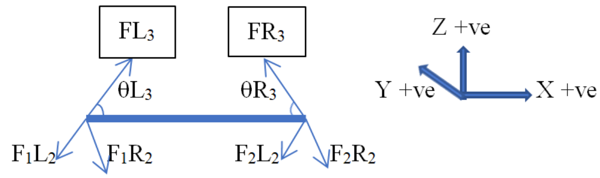

Figure 3. Free body diagram of spreader bar at level 3 with applied forces

$$FL_3 \cos(\theta L_3+\gamma_3) - FR_3 \cos(\theta R_3-\gamma_3) + \sin\delta_{12}[F_1R_2 \sin(\theta_1R_2-\gamma_{12}) + F_1L_2 \sin(\theta_1L_2+\gamma_{12})] - \sin\delta_{22}[F_2R_2 \sin(\theta_2R_2-\gamma_{22}) + F_2L_2 \sin(\theta_2L_2+\gamma_{22})] = 0 \tag{5}$$
$$FL_3 \sin(\theta L_3+\gamma_3) + FR_3 \sin(\theta R_3-\gamma_3) - \cos\delta_{12}[F_1R_2 \sin(\theta_1R_2-\gamma_{12}) + F_1L_2 \sin(\theta_1L_2+\gamma_{12})] - \cos\delta_{22}[F_2R_2 \sin(\theta_2R_2-\gamma_{22}) + F_2L_2 \sin(\theta_2L_2+\gamma_{22})] = 0 \tag{6}$$

Where θL_3 and θR_3 are the sling angles with the spreader bar SBL_3 at level 3; θ_1R_2 and θ_1L_2 are respectively the right and left sling angles at the second level in the left side plane; θ_2R_2 and θ_2L_2 are respectively the right and left sling angles at the second level in the right-side plane. The left and right-side planes are supported respectively by the left/right ends of the spreader bar at the 3rd level; δ_{12} and δ_{22} are the angles of the 2 side planes with the vertical plane. γ_{12}/γ_{22} and γ_3 are the slopes of the spreader bars at the second and third levels respectively. FL_3 and FR_3 are the left and right sling forces at the third level; F_1R_2/F_1L_2 and F_2R_2/F_2L_2 are respectively the right/left sling forces at the second level in respectively the left and right-side planes.

In Equation (5), the two terms $\sin\delta_{12}[F_1R_2 \sin(\theta_1R_2-\gamma_{12}) + F_1L_2 \sin(\theta_1L_2+\gamma_{12})]$ and $\sin\delta_{22}[F_2R_2 \sin(\theta_2R_2-\gamma_{22}) + F_2L_2 \sin(\theta_2L_2+\gamma_{22})]$ represent the horizontal projections of the diagonal sling forces at the second level acting on the horizontal axis at the third level. These components are very small because the angles δ_{12} and δ_{22} are nearly zero, making their sines almost negligible. Additionally, these forces act in opposite directions on the spreader bar at level 3. Since keeping them in Equation (5) would complicate the calculation of FL_3 and FR_3 without significantly changing their final values, they were removed from the equation. So, Equation (5) will be expressed as (5').

$$FL_3 = FR_3 \cos(\theta R_3-\gamma_3)/\cos(\theta L_3+\gamma_3) \tag{5'}$$

By substituting FL_3 in Equation (6) to solve for FR_3 then solving for FL_3 in Equation (5'), Equations (7) and (8) will be obtained.

$$FR_3 = \frac{\{cos\delta_{12} *[F_1R_2 *sin(\theta_1R_2-\gamma_{12})+F_1L_2*sin(\theta_1L_2+\gamma_{12}]+cos\delta_{22}*[F_2R_2*sin(\theta_2R_2-\gamma_{22})+F_2L_2*sin(\theta_2L_2+\gamma_{22})]\}*cos(\theta L3+\gamma_3)}{cos(\theta R_3-\gamma_3)+cos(\theta L_3+\gamma_3)*sin(\theta R_3-\gamma_3)} \quad (7)$$

$$FL_3 = \frac{\{cos\delta_{12} *[F_1R_2*sin(\theta_1R_2-\gamma_{12})+F_1L_2*sin(\theta_1L_2+\gamma_{12})]+cos\delta_{22}*[F_2R_2*sin(\theta_2R_2-\gamma_{22})+F_2L_2*sin(\theta_2L_2+\gamma_{22})]\}}{1+cos(\theta L_3+\gamma_3)*tan(\theta R_3-\gamma_3)} \quad (8)$$

In more complex systems with more than six lifting points, the traditional static equilibrium model becomes insufficient. The complexity of these systems, which involve multiple sling lengths, shackles, and spreader bars, requires more advanced methods to ensure that all forces are balanced and that the module remains stable throughout the lift. While static equilibrium analysis can still be applied to smaller systems, it becomes less reliable as the number of lifting points increases, particularly when the rigging system is subjected to dynamic forces ignored within the current study.

2.2 Designing Rigging Assemblies for Larger Configurations

For larger modular lifting configurations, such as those involving 8 or 16 lifting points, the traditional approach can still be extended by breaking down the larger system into smaller, more manageable sub-systems. However, with those employing a total of 12 or 14 lifting points composed of respectively a pair of 6-pick point segments or a pair of 6-pick point segments and a 2-pick point segment, the traditional model wouldn't be computationally accessible. In other words, it would fail to analyze the sling forces in the 12 or 14-pick point segments. Lastly, for the 10-pick point configuration composed of an 8-pick point and a 2-pick point segments, the method could still analyze the sling forces in the former segment. However, based on the design methodology adopted in MinayHashemi et al. [3], this step would be insufficient for selecting the 2-pick point segment components.

2.2.1 8-pick point configuration

An 8-point configuration can be divided into two 4-point rigging assemblies connected by a spreader bar at a higher lifting level. Each 4-point system is analyzed separately, and the total load is transferred to the spreader bar at level 4 (Figure 4).

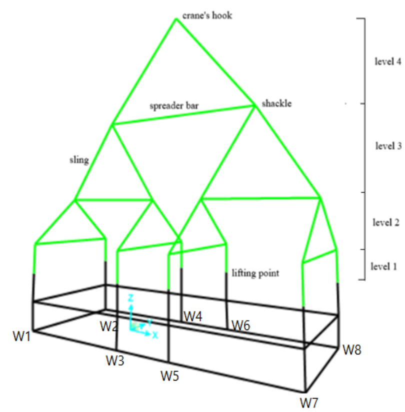

Figure 4. 3D schematic of an 8-pick point rigging assembly

The left segment (W_1 to W_4) and the right segment (W_5 to W_8) each transfer their respective forces to the spreader bar, which then distributes the total load up to the crane's hook. Using the same methodology and equations from the previous section, Equations (9), (10), (11), and (12) can be derived to calculate the forces in respectively the left- and right-side assembly. Equilibrium equations applied to the free-body diagram of the spreader bar at level 4 shown in Figure 5 will yield the sling forces F_{R4} and F_{L4} expressed in Equations (13) and (14) respectively.

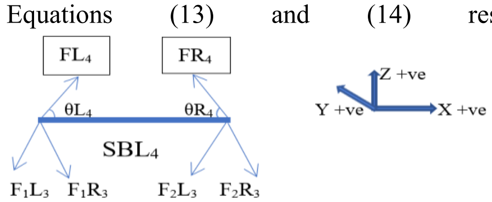

Figure 5. Free body diagram of spreader bar at level 4

$$F_1R_3 = \frac{\{cos\delta_{12} *[F_1R_2*sin(\theta_1R_2-\gamma_{12})+F_1L_2*sin(\theta_1L_2+\gamma_{12})]+cos\delta_{22}*[F_2R_2*sin(\theta_2R_2-\gamma_{22})+F_2L_2*sin(\theta_2L_2+\gamma_{22})]\}*cos(\theta_1L_3+\gamma_{13})}{cos(\theta_1R_3-\gamma_{13})+cos(\theta_1L_3+\gamma_{13})*sin(\theta_1R_3-\gamma_{13})} \quad (9)$$

$$F_1L_3 = \frac{\{cos\delta_{12} *[F_1R_2*sin(\theta_1R_2-\gamma_{12})+F_1L_2*sin(\theta_1L_2+\gamma_{12})]+cos\delta_{22}*[F_2R_2*sin(\theta_2R_2-\gamma_{22})+F_2L_2*sin(\theta_2L_2+\gamma_{22})]\}}{1+cos(\theta_1L_3+\gamma_{13})*tan(\theta_1R_3-\gamma_{13})} \quad (10)$$

$$F_2R_3 = \frac{\{cos\delta_{32} *[F_3R_2*sin(\theta_3R_2-\gamma_{32})+F_3L_2*sin(\theta_3L_2+\gamma_{32})]+cos\delta_{42}*[F_4R_2*sin(\theta_4R_2-\gamma_{42})+F_4L_2*sin(\theta_4L_2+\gamma_{42})]\}*cos(\theta_2L_3+\gamma_{23})}{cos(\theta_2R_3-\gamma_{23})+cos(\theta_2L_3+\gamma_{23})*sin(\theta_2R_3-\gamma_{23})} \quad (11)$$

$$F_2L_3 = \frac{\{cos\delta_{32} *[F_3R_2*sin(\theta_3R_2-\gamma_{32})+F_3L_2*sin(\theta_3L_2+\gamma_{32})]+cos\delta_{42}*[F_4R_2*sin(\theta_4R_2-\gamma_{42})+F_4L_2*sin(\theta_4L_2+\gamma_{42})]\}}{1+cos(\theta_2L_3+\gamma_{23})*tan(\theta_2R_3-\gamma_{23})} \quad (12)$$

$$FR_4 = \{(cos\delta_{12}\ [F_1R_2sin\ (\theta_1R_2 - \gamma_{12}) + F_1L_2sin(\theta_1L_2 + \gamma_{12})] + cos\delta_{22}\Big[F_2R_2sin(\theta_2R_2 - \gamma_{22}) + F_2L_2sin(\theta_2L_2 + \gamma_{22})]\left(\frac{sin(\theta_1R_3+\theta_1L_3)}{[1+cos(\theta_1L_3+\gamma_{13})sin(\theta_1R_3-\gamma_{13})]}\right) + (cos\delta_{32}\ [F_3R_2sin\ (\theta_3R_2 - \gamma_{32}) + F_3L_2sin(\theta_3L_2 + \gamma_{32})\Big] + cos\delta_{42}[F_4R_2sin(\theta_4R_2 - \gamma_{42}) + F_4L_2sin(\theta_4L_2 + \gamma_{42})]]\left(\frac{sin(\theta_2R_3+\theta_2L_3)}{[1+cos(\theta_2L_3+\gamma_{23})tan(\theta_2R_3-\gamma_{23})]\,cos(\theta_2R_3-\gamma_{23})}\right)\}\ \frac{cos(\theta L_4+\gamma_4)}{sin(\theta L_4+\theta R_4)} \tag{13}$$

$$FL_4 = \{(cos\delta_{12}\ [F_1R_2sin\ (\theta_1R_2 - \gamma_{12}) + F_1L_2sin(\theta_1L_2 + \gamma_{12})] + cos\delta_{22}\Big[F_2R_2sin(\theta_2R_2 - \gamma_{22}) + F_2L_2sin(\theta_2L_2 + \gamma_{22})]\left(\frac{sin(\theta_1R_3+\theta_1L_3)}{[1+cos(\theta_1L_3+\gamma_{13})sin(\theta_1R_3-\gamma_{13})]}\right) + (cos\delta_{32}\ [F_3R_2sin\ (\theta_3R_2 - \gamma_{32}) + F_3L_2sin(\theta_3L_2 + \gamma_{32})\Big] + cos\delta_{42}[F_4R_2sin(\theta_4R_2 - \gamma_{42}) + F_4L_2sin(\theta_4L_2 + \gamma_{42})]]\left(\frac{sin(\theta_2R_3+\theta_2L_3)}{[1+cos(\theta_2L_3+\gamma_{23})tan(\theta_2R_3-\gamma_{23})]\,cos(\theta_2R_3-\gamma_{23})}\right)\}\ \frac{cos(\theta R_4-\gamma_4)}{sin(\theta L_4-\theta R_4+2\gamma_4)} \tag{14}$$

2.2.2 10-pick point configuration

A 10-point system can be analyzed by combining an 8-point assembly with a 2-point segment (Figure 6).

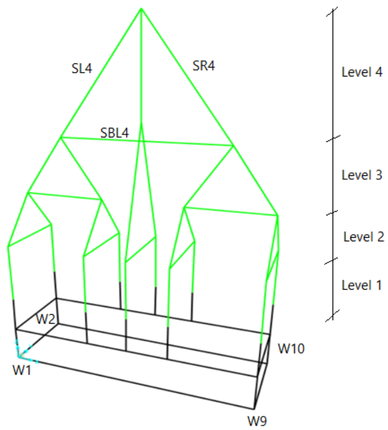

Figure 6. 3D schematic of a 10-pick point rigging assembly

The 2-point system, located in the center of the rigging setup, handles a smaller portion of the load. The analysis of the 8-point system is carried out as described in the previous section, but the 2-point system, which has a different structural design, requires additional consideration. Unlike the 8-point system, the 2-point segment is less complex, consisting of fewer lifting points and levels. The challenge lies in ensuring that the 2-point system, which has fewer lifting points, does not lead to uneven distribution of forces when combined with the larger 8-point system. Based on that, its structural design was conducted following that of the 8-point segment on a level-to-level basis.

Previous work by MinayHashemi et al. [3] did not include an in-depth structural analysis of the 2-point segment and assumed identical sling lengths across both the 2-point and 4-point segments in a 6-pick point configuration. However, this assumption becomes problematic when the 2-point segment differs in terms of the number of levels compared to the 8-point segment. For accurate rigging design, it is essential to carefully analyze the 2-point configuration and adjust for the different levels in the system.

2.2.3 12-pick point configuration

A 12-point system consists of two 6-point assemblies; each designed using the principles applied in the 4-point configuration. The total weight of the module is transferred to a spreader bar located at the fourth level, which ensures an even distribution of forces across all the lifting points (Figure 7).

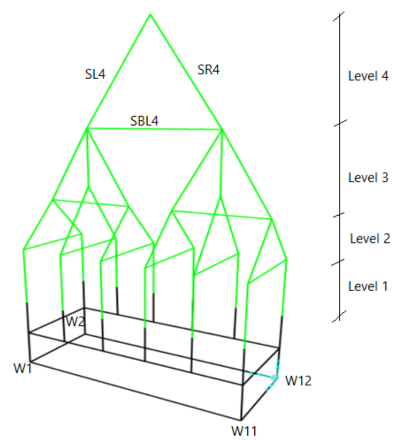

Figure 7. 3D schematic of a 12-pick point rigging assembly

Each 6-point assembly is analyzed independently, with the forces from the left and right segments being transferred to the spreader bar. In this case, when analyzing the forces acting on the spreader bar at level 4 in the XZ plane, four unknown force components need to be determined for each end of the spreader bar as shown in Figure 8. FL_4 and FR_4 are respectively the left and right sling forces at the fourth level of the rigging assembly; θL_4 and θR_4 are respectively the left and right sling angles with the spreader bar SBL_4 at the fourth level; F_1M_3 and F_2M_3 are respectively the left- and right-middle sling forces at the third level supported by the left and right spreader bar ends at level 4 of the rigging assembly. By applying equilibrium, Equations (15) and (16) are obtained.

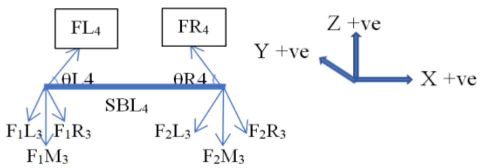

Figure 8. Free body diagram of spreader bar at level 4 for a 12-pick point configuration

$$FL_{4X} - FR_{4X} - F_1L_{3x} + F_1R_{3x} - F_2L_{3x} + F_2R_{3x} = 0 \quad (15)$$

$$FL_{4Z} + FR_{4Z} - F_1L_{3z} - F_1R_{3z} - F_2L_{3z} - F_2R_{3z} - F_1M_3 - F_2M_3 = 0 \quad (16)$$

F_1L_3 and F_1R_3 are the sling forces on the left side, and F_2L_3 and F_2R_3 are the sling forces on the right side of the spreader bar SBL_4 were already computed in the 8-pick point rigging assembly analysis section in this paper. F_1M_3 and F_2M_3 are the 2 additional forces applying vertically downwards due to the presence of the 2-pick point segments. This will lead to a system of 2 variables (FL_{4x} and FR_{4x}) in the X direction and 4 variables (FL_{4z}, FR_{4z}, F_1M_3, and F_2M_3) in the Z direction. Having only 2 equations to solve such a system will jeopardize reaching a solution.

While static equilibrium can be used to analyze the 6-point assemblies, the complexity increases at the fourth level, where the spreader bar introduces additional unknowns. These unknowns can't be easily solved using static equilibrium methods alone, and therefore, finite element analysis (FEA) could be employed to accurately model the forces in the system. The additional level of complexity requires a more robust approach to ensure stability and accurate force distribution calculations.

2.2.4 14 pick-point segments

A 14-point system includes both a 12-point assembly and a 2-point assembly (Figure 9). The design for the 12-point segment follows the same principles outlined above, but the 2-point segment introduces a new challenge. The 2-point system, located in the middle of the rigging assembly, consists of fewer lifting points and levels, which complicates the design process. MinayHashemi et al. [3] assumed that the rigging configuration of the 2-point segment matched the number of levels in the 4-point system, but this assumption is no longer valid in this case.

To design the 2-pick point system, a more advanced method involving its analysis should be applied. A new method for selecting rigging components is necessary. This method should account for the differing number of levels in the system compared to the 12-point segment and ensure that the forces are balanced and stable. The 2-point system must be analyzed independently of the 12-point segment and integrated into the overall rigging design.

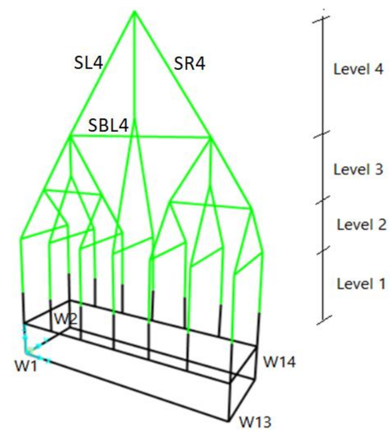

Figure 9. 3D schematic of a 14-pick point rigging assembly

2.2.5 16 pick-point segments

A 16-point configuration is one of the most complex systems used for large modular lifts. It consists of two 8-point assemblies, with a spreader bar and two diagonal slings at the fifth level (Figure 10).

Similar to the 8-point configuration, each 8-point segment is analyzed independently using the methods from Section 2.2.1. However, with the addition of a fifth level of rigging components, the spreader bar introduces new forces that must be carefully analyzed. In this case, the forces at level 5 must be determined through a free-body diagram of the spreader bar in the XZ plane, which will have unknowns in both the vertical and horizontal directions (Figure 11). Considering the equations already derived from section **2.2.1** for F_1R_4 (Equation 17) and F_1L_4 (Equation 18) in the left 8-pick point segment; and similarly those for F_2R_4 (Equation 19) and F_2L_4 (Equation 20) in the right 8-pick point segment; and by applying equilibrium, Equations (21) and (22) were obtained. And by solving the system of these 2 equations, FL_5 and FR_5 were determined in Equations (23) and (24) respectively with the integration of Equations (25) and (26) for simplicity.

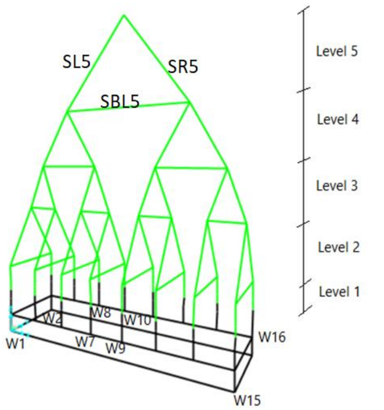

Figure 10. 3D schematic of a 16-pick point rigging assembly

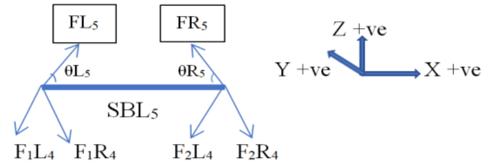

Figure 11. Free body diagram of spreader bar at level 5 with applied forces

The analysis for the 16-point system remains similar to the 8-point and 12-point configurations, but the additional level introduces complexity. To ensure the accuracy of the design, finite element analysis (FEA) should be used to model the forces acting on the system at this level. This advanced analysis will ensure that all components are properly designed and the forces are balanced throughout the system.

$$F_1R_4=\{(\cos\delta_{12}[F_1R_2\sin(\theta_1R_2-\gamma_{12})+F_1L_2\sin(\theta_1L_2+\gamma_{12})]+\cos\delta_{22}[F_2R_2\sin(\theta_2R_2-\gamma_{22})+F_2L_2\sin(\theta_2L_2+\gamma_{22})])((\sin(\theta_1R_3+\theta_1L_3))/([1+\cos(\theta_1L_3+\gamma_{13})\sin(\theta_1R_3-\gamma_{13})]))+(\cos\delta_{32}[F_3R_2\sin(\theta_3R_2-\gamma_{32})+F_3L_2\sin(\theta_3L_2+\gamma_{32})]+\cos\delta_{42}[F_4R_2\sin(\theta_4R_2-\gamma_{42})+F_4L_2\sin(\theta_4L_2+\gamma_{42})])((\sin(\theta_2R_3+\theta_2L_3))/(\cos(\theta_2R_3-\gamma_{23})[1+\cos(\theta_2L_3+\gamma_{23})\tan(\theta_2R_3-\gamma_{23})]))\}\cos(\theta_1L_4+\gamma_{14})/\sin(\theta_1L_4+\theta_1R_4) \tag{17}$$

$$F_1L_4=\{(\cos\delta_{12}[F_1R_2\sin(\theta_1R_2-\gamma_{12})+F_1L_2\sin(\theta_1L_2+\gamma_{12})]+\cos\delta_{22}[F_2R_2\sin(\theta_2R_2-\gamma_{22})+F_2L_2\sin(\theta_2L_2+\gamma_{22})])((\sin(\theta_1R_3+\theta_1L_3))/([1+\cos(\theta_1L_3+\gamma_{13})\sin(\theta_1R_3-\gamma_{13})]))+(\cos\delta_{32}[F_3R_2\sin(\theta_3R_2-\gamma_{32})+F_3L_2\sin(\theta_3L_2+\gamma_{32})]+\cos\delta_{42}[F_4R_2\sin(\theta_4R_2-\gamma_{42})+F_4L_2\sin(\theta_4L_2+\gamma_{42})])((\sin(\theta_2R_3+\theta_2L_3))/(\cos(\theta_2R_3-\gamma_{23})[1+\cos(\theta_2L_3+\gamma_{23})\tan(\theta_2R_3-\gamma_{23})]))\}\cos(\theta_1R_4-\gamma_{14})/\sin(\theta_1L_4-\theta_1R_4+2\gamma_{14}) \tag{18}$$

$$F_2R_4=\{(\cos\delta_{12}[F_1R_2\sin(\theta_1R_2-\gamma_{12})+F_1L_2\sin(\theta_1L_2+\gamma_{12})]+\cos\delta_{22}[F_2R_2\sin(\theta_2R_2-\gamma_{22})+F_2L_2\sin(\theta_2L_2+\gamma_{22})])((\sin(\theta_1R_3+\theta_1L_3))/([1+\cos(\theta_1L_3+\gamma_{13})\sin(\theta_1R_3-\gamma_{13})]))+(\cos\delta_{32}[F_3R_2\sin(\theta_3R_2-\gamma_{32})+F_3L_2\sin(\theta_3L_2+\gamma_{32})]+\cos\delta_{42}[F_4R_2\sin(\theta_4R_2-\gamma_{42})+F_4L_2\sin(\theta_4L_2+\gamma_{42})])((\sin(\theta_2R_3+\theta_2L_3))/(\cos(\theta_2R_3-\gamma_{23})[1+\cos(\theta_2L_3+\gamma_{23})\tan(\theta_2R_3-\gamma_{23})]))\}\cos(\theta_2L_4+\gamma_{24})/\sin(\theta_2L_4+\theta_2R_4) \tag{19}$$

$$F_2L_4=\{(\cos\delta_{12}[F_1R_2\sin(\theta_1R_2-\gamma_{12})+F_1L_2\sin(\theta_1L_2+\gamma_{12})]+\cos\delta_{22}[F_2R_2\sin(\theta_2R_2-\gamma_{22})+F_2L_2\sin(\theta_2L_2+\gamma_{22})])((\sin(\theta_1R_3+\theta_1L_3))/([1+\cos(\theta_1L_3+\gamma_{13})\sin(\theta_1R_3-\gamma_{13})]))+(\cos\delta_{32}[F_3R_2\sin(\theta_3R_2-\gamma_{32})+F_3L_2\sin(\theta_3L_2+\gamma_{32})]+\cos\delta_{42}[F_4R_2\sin(\theta_4R_2-\gamma_{42})+F_4L_2\sin(\theta_4L_2+\gamma_{42})])((\sin(\theta_2R_3+\theta_2L_3))/(\cos(\theta_2R_3-\gamma_{23})[1+\cos(\theta_2L_3+\gamma_{23})\tan(\theta_2R_3-\gamma_{23})]))\}\cos(\theta_2R_4-\gamma_{24})/\sin(\theta_2L_4-\theta_2R_4+2\gamma_{24}) \tag{20}$$

$$FL_5\cos(\theta L_5+\gamma_5)-FR_5\cos(\theta R_5-\gamma_5)+F_1R_4\cos(\theta_1R_4-\gamma_{14})-F_1L_4\cos(\theta_1L_4+\gamma_{14})+F_2R_4\cos(\theta_2R_4-\gamma_{24})-F_2L_4\cos(\theta_2L_4+\gamma_{24})=0 \tag{21}$$

$$FL_5\sin(\theta L_5+\gamma_5)+FR_5\sin(\theta R_5-\gamma_5)-(F_1L_4\sin(\theta_1L_4-\gamma_{14})-F_1R_4\sin(\theta_1R_4-\gamma_{14})-F_2R_4\sin(\theta_2R_4-\gamma_{24})-F_2L_4\sin(\theta_2L_4+\gamma_{24})=0 \tag{22}$$

$$FL_5=\frac{c_2\cos(\theta R_5-\gamma_5)+c_1\sin(\theta R_5-\gamma_5)}{\sin(\theta L_5+\theta R_5)} \tag{23}$$

$$FR_5=\frac{c_2\cos(\theta R_5-\gamma 5)\cos(\theta L_5+\gamma_5)+c_1\sin(\theta R_5-\gamma_5)\cos(\theta L_5+\gamma_5)-C1\sin(\theta L_5+\theta R_5)}{\cos(\theta R_5-\gamma_5)\sin(\theta L_5+\theta R_5)} \tag{24}$$

FL_5 and FR_5 are respectively the left and right sling forces at the fifth level of the rigging assembly; θL_5 and θR_5 are respectively the left and right sling angles with the spreader bar SBL_5 at the fifth level; γ_5 is the slope of the spreader bar at the fifth level. c_1 and c_2 are combinations of constants given in Equations (25) and (26).

$$c_1 = -(F_1R_4 \cos(\theta_1 R_4 - \gamma_{14}) - F_1L_4 \cos(\theta_1 L_4 + \gamma_{14}) + F_2R_4 \cos(\theta_2 R_4 - \gamma_{24}) - F_2L_4 \cos(\theta_2 L_4 + \gamma_{24}) \quad (25)$$

$$c_2 = F_1L_4 \sin(\theta_1 L_4 + \gamma_{14}) + (F_1R_4 \sin(\theta_1 R_4 - \gamma_{14}) + F_2L_4 \sin(\theta_2 L_4 + \gamma_{24}) + F_2R_4 \sin(\theta_2 R_4 - \gamma_{24}) \quad (26)$$

3 Conclusion

This study has explored the limitations of the static equilibrium method in designing rigging systems for modular lifting configurations with more than 6 lifting points ignored in previous studies. While static equilibrium is effective for smaller configurations, it becomes less reliable for systems with more than six lifting points, where additional techniques, such as finite element analysis (FEA), could be required. The findings provide a framework for designing rigging assemblies for larger modular systems, offering insights into how to precisely and efficiently balance forces and ensure stability during lifting operations.

Despite not being the ideal method for analyzing large rigging configurations, the verification process confirmed, through a detailed mathematical computation process, that static equilibrium methods are still valid for configurations like 8-point and 16-point systems despite the need for successive analyses. However, this process is: *(i)* tedious because it takes time to perform analysis calculations for each level and proceed to the next higher one(s); *(ii)* error-prone since any error in the earlier steps of calculation would be carried forward to higher levels which would lead to design and selection inaccuracies; and *(iii)* limited to sling force computations only excluding those for spreader bars and other rigging components. On the other hand, for other configurations, particularly the 10-point and 14-point systems, the method becomes less effective due to the complexity of the force distribution and the non-matching number of levels. Moreover, the method becomes invalid with the 12-pick point system due to having more unknowns than equations.

This study presents a hands-on insight to introduce a new comprehensive rigging design methodology that: (i) computes the sling angles and sling length justifications to establish equilibrium of rigging arrangements with 6 or more lifting points. (ii) simplifies the structural analysis by applying simultaneous solutions (with the help of structural analysis software preferably applying the FEA method), instead of systematic or successive analyses based on level-to-level free-body diagrams which are time-wasting, error-prone, and invalid for all n-pick point configurations. (iii) has the potential to account for not only static loads as in the existing studies, but also address dynamic effects (i.e., forces and stresses) associated with the lifted modules such as wind loading and dynamic vibrations, in addition to the module's deformations.

References

[1] H. Taghaddos, U. Hermann, and A. Abbasi. Automated crane planning and optimization for modular construction. *Automation in Construction, 95*, 219-232, 2018.

[2] J. Cho, K. Lee, and H. Lee. Impact analysis of the new OSHA cranes and derricks regulations on crane operation safety. *KSCE Journal of Civil Engineering, 21*(1), 54-66, 2017.

[3] S. MinayHashemi, S. Han, J. Olearczyk, A. Bouferguene, M. Al-Hussein, and J. Kosa. Automated rigging design for heavy industrial lifts. *Automation in Construction, 112*, 103083, 2020.

[4] Institute, A. P. (2000). API RP2A: Recommended Practice for Planning, Designing, and Constructing Fixed Offshore Platforms-Working Stress Design: Upstream Segment. API Recommended Practice 2A-WSD (RP 2A-WSD): Errata and Supplement 1, December 2002: *American Petroleum Institute*.

[5] Veritas, D. N. Guideline for offshore structural reliability analysis: application to jacket platforms. *Det Norske Veritas,* 1996.

[6] J. W. Bunce and T. A. Wyatt. Development of unified design criteria for heavy lift operations offshore. In *Proceedings of the Offshore Technology Conference*, OTC-4190-MS, Houston, Texas, 1982.

[7] K. Sam. Offshore heavy lift rigging analysis using spreadsheet. *Practice Periodical on Structural Design and Construction*, 14(2), 63-69, 2009.

[8] C. Crull. Direct determination of sling tensions in heavy rigging. In *Proceedings of the Offshore Technology Conference*, OTC-6395-MS, Houston, Texas, 1990.

[9] S. Hashemi, S. Han, J. Olearczyk, A. Bouferguene, M. Al-Hussein and J. Kosa. Automated mathematical-based design framework for the selection of rigging configuration. In *Proceedings of the 36th ISARC*, pages 172-178, Banff, Canada, 2019.

[10] J. Olearczyka, M. Kainata, J. Kosab, S. Adeeba, and M. Al-Husseina. Heavy lift rigging algorithm for construction operation (*iRigging),* 2015.